

Percolation and spatial correlations in a two-dimensional continuum deposition model

J. Asikainen^{1,*} and T. Ala-Nissila^{1,2}

¹*Helsinki Institute of Physics and Laboratory of Physics, Helsinki University of Technology,
P.O. Box 1100, FIN-02015 HUT, Espoo, Finland*

²*Department of Physics, Brown University, Providence, Rhode Island 02912*

(Received 8 June 1999)

We introduce a two-dimensional continuum deposition model of spatially extended objects, with an effective repulsive contact interaction between them represented by a parameter $0 \leq q \leq 1$. For $q=0$, the deposited network is uniformly random, while for $q=1$ particles are not allowed to overlap. For $0 \leq q < 1$, we carry out extensive simulations on fibers, needles, and disks to study the dependence of the percolation threshold on q . We derive expressions for the threshold near $q=0$ and $q=1$ and find good qualitative agreement with the simulations. The deposited networks produced by the model display nontrivial density correlations near percolation threshold. These are reflected in the appropriate spatial correlation functions. We study such functions close to $q=1$ and derive an approximate expression for the pair distribution function.

PACS number(s): 64.60.Ak, 02.70.-c, 61.43.Hv

I. INTRODUCTION

There are various deposition phenomena in nature where transport mechanisms bring particles to a surface. These include deposition of colloidal, polymer, and fiber particles [1–7]. In some cases, such deposition phenomena involve particles whose size is large compared to their mutual interaction range, and so the main deposition mechanism is due to particle exclusion. Among the most studied in this class are the random and cooperative sequential adsorption models [1,2]. There particles are deposited on a surface and either stick or are rejected according to certain exclusion rules, with a maximum coverage (the “jamming limit”) less than unity. These types of models should be contrasted with the case of multilayer surface growth [1,6–8], where the main focus is on the asymptotic behavior of the growing surface in the continuum limit [9].

A particularly interesting example involving particle deposition can occur in the case of colloidal suspensions. For some such systems, the interparticle repulsion is strong enough to prevent multilayer growth [3]. However, the existence of dispersion forces can change this repulsion so that even particle aggregation and subsequent precipitation out of the suspension may occur [7,10]. For larger particles or clusters of particles, gravity must also be taken into account and can in part help to overcome interparticle repulsion. Experiments reveal that, e.g., sedimentation produces nontrivial spatial structures [11]. A full microscopic treatment of many deposition processes such as sedimentation is a formidable task [12]. Because of this, phenomenological deposition models may be useful in studying how various effective interactions influence the mass density distributions of the consequent deposits.

In addition to their practical applications, two-dimensional (2D) random deposition models have been the topic of intense study in their own right. In particular, they

have been extensively studied in the context of continuum percolation theory [13–28]. These models have included uniformly random networks of various objects as well as hard- and soft-core interactions between the constituent particles. The quantity of central importance in these studies is the percolation threshold or critical particle density which for permeable objects can be related to the excluded volume of the particles [19]. This quantity depends on the geometrical shape of the deposited particles as well as on interactions between them in a nontrivial way.

In this paper, we present a study of the percolation properties and spatial correlations in networks formed by a simple 2D deposition model. In the model, there is an effective contact repulsion between the deposited particles, which can be tuned from no repulsion (uniformly random networks) to a strict nonoverlap case (the random sequential adsorption limit). This model is complementary to the recently introduced “floculation model,” where there is enhanced clustering of deposited objects [27–30]. We study the percolation thresholds of widthless needles, fibers of finite width, and disks. We derive analytic approximations for the thresholds in the appropriate limits. Furthermore, we study spatial correlations in the model through the appropriate correlation functions, and derive an expression for the pair distribution function.

II. DEFINITION OF THE MODEL

The model studied here, called the “rejection model” (RM), was originally introduced by Åström [29]. In the RM, spatially extended objects are sequentially deposited on a 2D plane in continuum. Both the orientation of the object and its spatial coordinates are chosen from a uniformly random distribution. If a deposited object lands on empty space, the attempt is always accepted. However, if it lands on another object already on the surface, the attempt is rejected with a given probability $0 \leq q \leq 1$. Thus, the parameters that characterize the model are the rejection probability q , the dimensions of the deposited objects, the linear dimension L of the surface, and the number of deposited objects kept, N (i.e., the

*Author to whom correspondence should be addressed. Electronic address: Joonas.Asikainen@hut.fi

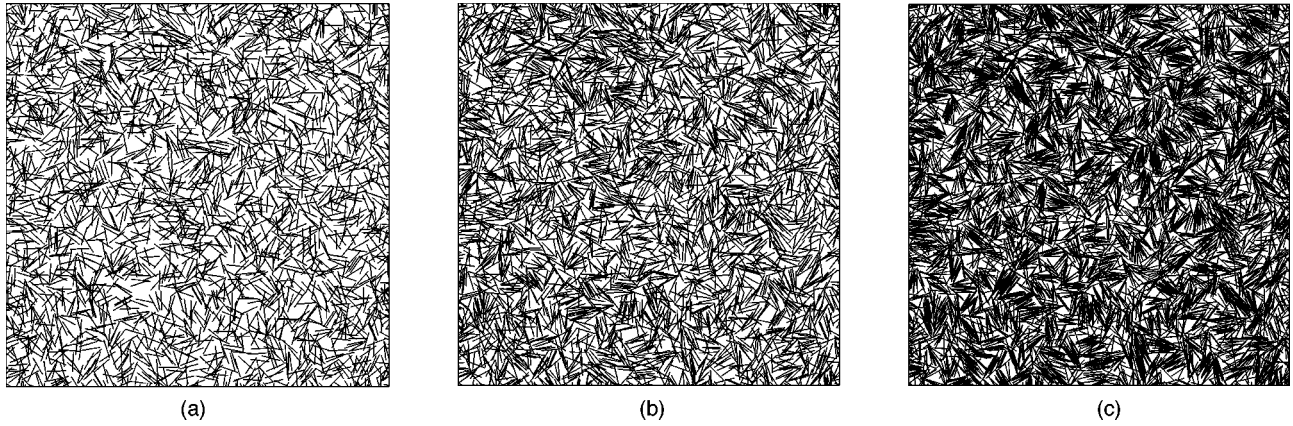


FIG. 1. Snapshot of networks of needles of length $\lambda=1$ close to the percolation threshold ($L=20$), for (a) $q=0.9$ ($N=2648$), (b) $q=0.99$ ($N=3616$), and (c) $q=0.999$ ($N=6332$).

number of accepted attempts).

In the limit $q=0$ the model reduces to the extensively studied case of a uniformly random network [4,13–17,23,27,28,31]. However, for $q>0$ there is an effective contact repulsion between the particles that tends to prevent overlaps. In particular, for the extreme case of $q=1$, a strict nonoverlap condition is imposed. This is the well-known limit of random sequential adsorption (RSA) models [1]. In this case, percolation with connectivity defined through particle overlaps is not possible, and deposition typically terminates to a finite density called the “jamming limit.”

Motivation for the model arises in part from deposition of particles such as large charged molecules on surfaces which tend to repel each other. Changing the parameter q allows the tuning of the effective contact repulsion between such particles. The RM is complementary to the flocculation model (FM), where the tendency of deposited particles to overlap is *enhanced* by a parameter $0 \leq p \leq 1$ [27,28,32]. For $p=0$, only a single connected cluster grows in the FM, while the rejection and flocculation models become equivalent to the uniformly random case for $p=1$ and $q=0$, respectively.

III. PERCOLATION PROPERTIES OF THE MODEL

When enough particles are deposited in a finite system, its edges become connected and percolation takes place in the model. The properties of the corresponding *continuum percolation transition* are of particular interest [19,33]. Indeed, continuum percolation of 2D rectangles [13,16,27,28], disks [13,14,16,18,19,21,22,26–28], and needles [13,15–17,23,27,28,31] among other geometric objects has been extensively studied, and the corresponding critical densities determined numerically. In this section, we present results of numerical and analytic calculations of the percolation properties of the RM for $0 \leq q < 1$ and compare the uniformly random limit $q=0$ with the existing studies [23,27,28].

A. Numerical results

We first present results of extensive numerical simulations of the critical densities of percolation $\eta_c(q)$ as a function of q for three different types of objects: needles of length λ , fibers (rectangles) of length λ and width ω (λ

$> \omega$), and disks of radius r_d . In each case, the system contains an inner box of length L and an outer box of length $L+L'$, with free boundary conditions. The size of the outer box is chosen so that the average density across the system is constant within the inner box [34]. The centers of the objects are distributed within the outer box. However, only objects partially or completely within the inner box are allowed to belong to the connected clusters. To keep track of the clusters we have employed the cluster multiple labeling technique [35] applied in the continuum case where any number of intersecting neighbors is allowed. In our final analysis, only one-sided percolation data were used.

The critical densities $\eta_c(q)$ were obtained by depositing a fixed number of objects N for a given system size L and checking for percolation. This was repeated for increasing values of N in the proper range of the particle density $\eta = N/L^2$. In this way, the whole curve of spanning probabilities was obtained for each system size L . The point where two such curves for any different system sizes intersect (the fixed point) gives an approximate value for $\eta_c = N_c/L^2$. We obtained these points by fitting the curves to error functions. The estimates thus obtained were extrapolated and the final values of $\eta_c(q)$ obtained using the standard Monte Carlo renormalization group (MCRG) method [21,36], with the smallest system studied being the reference system. For completeness, we also evaluated the correlation length exponent ν for our model from the MCRG procedure. In all cases studied here, we find that it is consistent with the universal value of $4/3$, as in lattice percolation [19,33].

1. Needles

Typical configurations generated by the model are shown in Figs. 1(a)–(c) for needles of unit length at the percolation threshold for various values of q . Employing the MCRG procedure for 100–500 ensembles and for system sizes $L=10,20,30,40,60$, with $0.0 \leq q \leq 0.999$ we obtain the values for $\eta_c(q)$ as displayed in Fig. 2. The curve displays interesting behavior in the two limits $q \rightarrow 0$ and $q \rightarrow 1$. First, $\eta_c(q)$ approaches the limit $q \rightarrow 0$ approximately linearly. Second, the expected divergence of $\eta_c(q)$ in the limit $q \rightarrow 1$ is clearly visible. Our best estimate for $\eta_c(0) = 5.59 \pm 0.05$ agrees well with other numerical studies reported in the literature for the uniformly random case (see, e.g., Refs. [23,27]). In addition

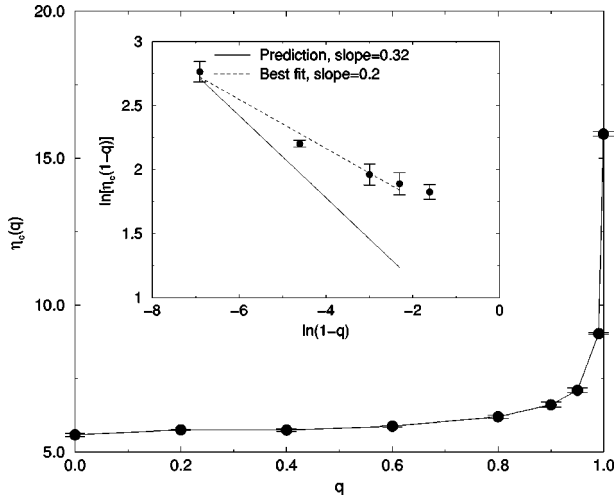


FIG. 2. The percolation threshold $\eta_c(q)$ vs q for a network of needles of length $\lambda = 1$. Inset shows the behavior near $q = 1$.

to the numerical estimates, $\eta_c(0)$ can be approximately determined by using the excluded volume arguments of Ref. [16], where $\eta_c(0)\langle A \rangle = \text{const} \approx 3.57$, and the excluded volume $\langle A \rangle = 0.637$ [37], which gives $\eta_c(0) \approx 5.61$.

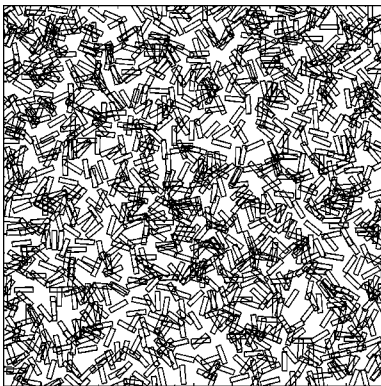
2. Fibers

In the case of fibers, we have used objects with an aspect ratio of $\lambda/\omega = 4/1$. Typical networks generated are shown in Figs. 3(a)–3(c) at the threshold for various values of q . Following the procedure employed for needles for system sizes $L = 10, 20, 40, 80$, and $0.0 \leq q \leq 0.999$ we obtain the $\eta_c(q)$ curve as shown in Fig. 4. These results have been obtained by averaging over 100–500 ensembles. In this case, there is no divergence of $\eta_c(q)$ in the limit $q \rightarrow 1$. We shall discuss this later in Sec. III B.

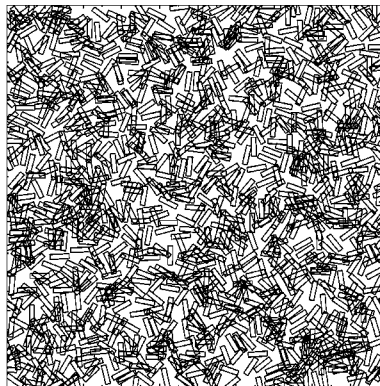
Our best estimate for the $q=0$ limit is $\eta_c(0) = 2.74 \pm 0.03$. This agrees well with the value reported by Provatas *et al.* [27].

3. Disks

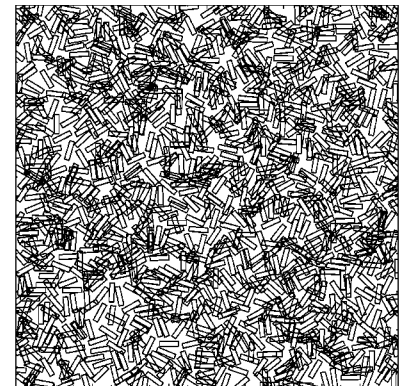
Typical networks of disks of radius $r_d = 1/2$ for various values of q at corresponding critical concentrations are shown in Figs. 5(a)–5(c). For disks we use the reduced num-



(a)



(b)



(c)

FIG. 3. Snapshot of networks of fibers with an aspect ratio $\lambda/\omega = 4$ close to the percolation threshold ($L = 20$), for (a) $q = 0.9$ ($N = 1148$), (b) $q = 0.99$ ($N = 1252$), and (c) $q = 0.999$ ($N = 1280$).

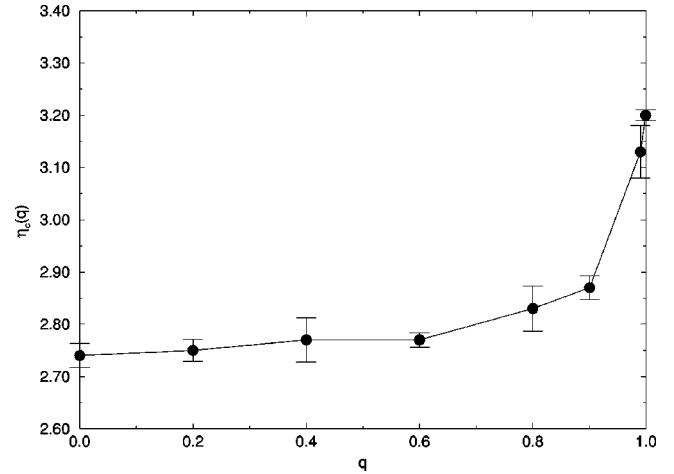


FIG. 4. The percolation threshold $\eta_c(q)$ vs q for a network of fibers of aspect ratio $\lambda/\omega = 4$.

ber density $\eta = Nr_d^2/L^2$. Using the MCRG procedure as explained above for system sizes $L = 10, 20, 40, 60, 80, 100$ and averaging over 10000 ensembles, we obtain the $\eta_c(q)$'s as shown in Fig. 6. Our best estimate for $\eta_c(0) = 0.36 \pm 0.01$ agrees within the errors with other numerical studies reported in the literature (see, e.g., Refs. [21,27]).

B. Analytic theory for percolation thresholds

1. The small q limit

We can qualitatively understand the behavior of the percolation thresholds for the two limits where $q \rightarrow 0$ and $q \rightarrow 1$ by using mean-field type arguments, similar to Ref. [27]. First, let us discuss the limit $q \rightarrow 0$. To this end, let us define r as the probability of a given object intersecting any other object in a uniformly random network ($q = 0$). This quantity depends on the dimensions of the object and the system size L . For example, in the case of fibers [38],

$$r = \frac{2(\lambda + \omega)^2}{\pi L^2} + \frac{2\lambda\omega}{L^2}. \quad (1)$$

Define $P^{(N)}$ to be the probability that the N th particle sticks on to the plane but not on any of the $N - 1$ previously

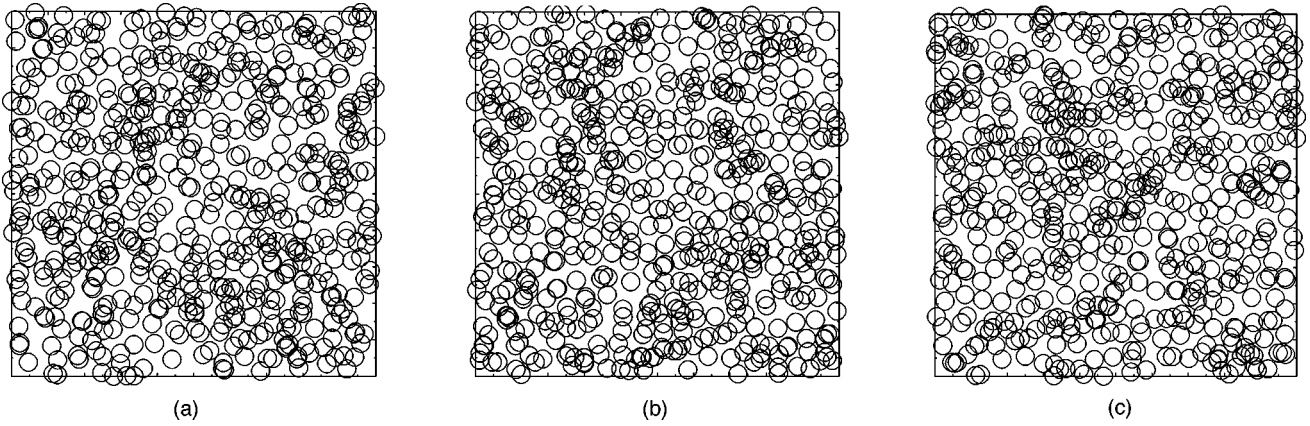


FIG. 5. Snapshot of networks of disks of radius $r_d=1/2$ close to the percolation threshold ($L=20$), for (a) $q=0.8$ ($N=580$), (b) $q=0.9$ ($N=584$), and (c) $q=0.99$ ($N=590$).

deposited particles. The probability that the first object sticks on the 2D plane is $P^{(1)}=1$. The probability that the second object sticks on to the plane but not on the first one is $P^{(2)}=(1-r)$. Continuing this for N particles, we find that $P^{(N)}=(1-r)^{N-1}$.

Consider next the uniformly random network of size L at its percolation threshold with $N_c=N_c(0)$ objects. The number of nonintersecting objects will be, on the average, $N_s=P^{(N_c)}N_c$. This estimate is accurate in the low density limit, but at high densities it overestimates the true N_s due to overlaps. The effect of $q>0$ is to increase the number of nonintersecting objects due to repulsion, but the backbone of the percolation cluster itself may be assumed to stay constant for $q\ll 1$. This implies that the percolation threshold increases. Since, on the average, a fraction q of the attempts to deposit an object are rejected, we estimate that the number of particles that can be added in such a way that they do not overlap with the percolation cluster is given approximately by q times the number of objects not belonging to the percolation cluster, to which a lower bound is qN_s . Therefore, at the percolation threshold for $q\leq 1$ we have

$$N_c(q)\geq N_c(0)+qN_s=N_c(0)+qP^{(N_c)}N_c(0). \quad (2)$$

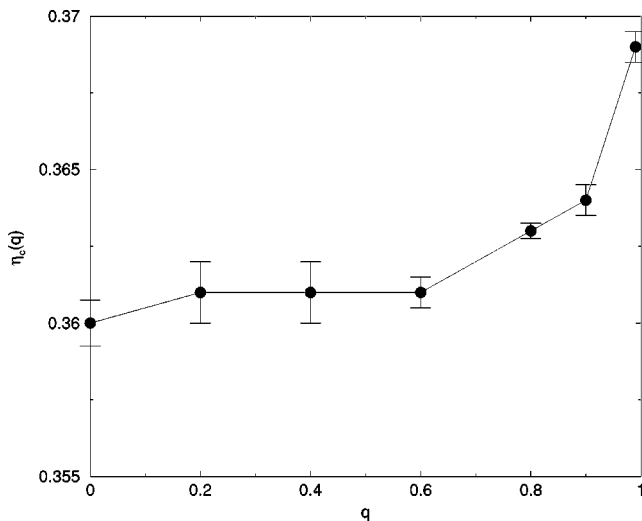


FIG. 6. The percolation threshold $\eta_c(q)$ vs q for a network of disks of radius $r_d=1/2$.

For the critical density we thus obtain

$$\eta_{c,L}(q)\geq \eta_{c,L}(0)+qP^{(N_c)}\eta_{c,L}(0)\equiv Aq+B, \quad (3)$$

where A and B are constants. Therefore, we can conclude that $\eta_{c,L}(q)$ increases linearly with q . This is also visible in our numerical data for the percolation thresholds. We can show that in the $L\rightarrow\infty$ limit the slope is given by

$$A=\eta_c(0)\exp\left[-\eta_c(0)\left(\frac{2(\lambda+\omega)^2}{\pi}+2\lambda\omega\right)\right]. \quad (4)$$

We have estimated the slope from numerical data and find that for needles $A=0.44$ while the lower bound of Eq. (4) gives $A=0.16$.

2. The divergence of the threshold for needles

The divergence of the percolation threshold for needles is to be expected since they have no area associated with them. Because of this they can be packed arbitrarily close to each other. From our data we find that the percolation threshold $\eta_c(q)$ diverges in the $q\rightarrow 1$ limit as $(1-q)^{-\nu}$, with $\nu\approx 0.20\pm 0.05$.

We can analytically estimate the divergence by using the results of Ziff and Vigil [39] in the RSA limit. They find by numerical simulations that the number of accepted attempts per unit area scales with the normalized number of adsorption attempts as $n(t)\propto t^x$, with $x\approx 0.32$, where $n=N\lambda/L^2$ and $t=T\lambda/L^2$ [40]. Here, N is the total number of accepted attempts and T is the total number of attempts.

If we consider the deposition process close to $q=1$, a total number of attempts $T_1\propto 1/(1-q)$ is needed before deposition of a single *overlapping* needle occurs. Using the results of Ref. [39], during this time approximately $n_s\approx T_1^x$ nonoverlapping needles are adsorbed. Assuming that $n_s\propto n$ and using the fact that $n=\eta$ (here $\lambda=1$), gives, close to percolation and in the limit $q\rightarrow 1$,

$$\eta_c(q)\propto \frac{1}{(1-q)^x}. \quad (5)$$

This result is in reasonably good agreement with our numerical data, although it is evident that we would need more data points closer to the limit $q = 1$ to more accurately obtain the scaling exponent.

In the cases of disks and fibers, the deposited objects have a finite area associated with them. In these cases, there is no divergence of $\eta_c(q)$. This is due to the finite jamming limit η_j in the RSA model, where the deposition process terminates since objects are not allowed to overlap. When more objects than this limit are deposited, the nonoverlap condition is violated, and thus there will eventually be spanning in the system. In fact, an upper bound for the percolation threshold for objects of finite area can be estimated by $\eta_c(q) \leq \eta_c(0) + \eta_j$ for all q .

IV. SPATIAL CORRELATION FUNCTIONS

In recent studies of the FM, nontrivial spatial correlations were found in the networks formed by deposition below and in the vicinity of the percolation threshold [27,28,32]. They manifest themselves in the radial pair distribution and mass density correlation functions. In this section, we present numerical and analytic results for spatial correlations in the RM for various values of q , and close to $q = 1$ in particular.

A. Pair distribution function

1. Needles

Consider the distribution of centers of mass of needles of unit length. The pair distribution function $\Omega(r)$ is defined through

$$\Omega(r)dr = \left\langle \frac{\text{Number of pairs of centers in a shell } (r, r+dr)}{\text{Total number of pairs of centers in system}} \right\rangle, \quad (6)$$

where the averaging is over all configurations. Let $\Delta N_{\text{CM}}(\vec{x}_i)$ be the number of centers of mass within the area element $\Delta A(\vec{x}_i)$ around the position vector \vec{x}_i . The number of pairs included in two different area elements is then given by the product $\Delta N_{\text{CM}}(\vec{x}_i)\Delta N_{\text{CM}}(\vec{x}_j)$. Further, the total number of pairs separated by vector \vec{x} in a given configuration is

$$\sum_{x_0} \Delta N_{\text{CM}}(\vec{x}_0)\Delta N_{\text{CM}}(\vec{x}_0 + \vec{x}). \quad (7)$$

Dividing this by $N(N-1)/2$ we obtain the probability of finding a pair of centers of mass separated by the vector \vec{x} in a given configuration. Multiplying and dividing by area elements yields

$$\Omega(r)dr = \frac{2}{N(N-1)} \left\langle \sum_{x_0} \frac{\Delta N_{\text{CM}}(\vec{x}_0)}{\Delta A(\vec{x}_0)} \frac{\Delta N_{\text{CM}}(\vec{x}_0 + \vec{x})}{\Delta A(\vec{x}_0 + \vec{x})} \times \Delta A(\vec{x}_0)\Delta A(\vec{x}_0 + \vec{x}) \right\rangle, \quad (8)$$

where we have assumed that the system is isotropic and thus Ω depends on $r \equiv |\vec{x}|$ only. The angular brackets denote configuration averaging. Taking the continuum limit where $\eta_{\text{CM}} = \lim_{\Delta A \rightarrow 0} (\Delta N_{\text{CM}}/\Delta A)$, we obtain

$$\Omega(r)dr = \frac{2}{N(N-1)} \left\langle \int_A d^2x_0 \eta_{\text{CM}}(\vec{x}_0) \times \eta_{\text{CM}}(\vec{x}_0 + \vec{x}) \Delta A(\vec{x}_0 + \vec{x}) \right\rangle. \quad (9)$$

Hence,

$$\Omega(r)dr = \frac{2}{N(N-1)} \int_A d^2x_0 G_{\text{CM}}(r_0, r) \Delta A(x_0 + x), \quad (10)$$

where

$$G_{\text{CM}}(r_0, r) \equiv \langle \eta_{\text{CM}}(\vec{x}_0) \eta_{\text{CM}}(\vec{x}_0 + \vec{x}) \rangle. \quad (11)$$

In Ref. [27], it is shown that for a uniformly random set of points with translational invariance this expression equals the exact pair distribution function Ω_a for a uniformly random network previously derived by Ghosh [4,41] as

$$\Omega_a(r, L) = \begin{cases} (4r/L^4)(\pi L^2/2 - 2rL + r^2/2) & \text{for } 0 \leq r \leq L \\ (4r/L^4)\{L^2[\arcsin(L/r) - \arccos(L/r)] \\ + 2L\sqrt{r^2 - L^2} - \frac{1}{2}(r^2 + 2L^2)\} & \text{for } L \leq r \leq \sqrt{2}L. \end{cases} \quad (12)$$

In Fig. 7(a) we show this function together with our numerical results of the pair distribution function of Eq. (8) for various values of q . The remarkable result is that within the numerical errors there is no dependence on q . This can be explained as follows. For $q > 0$, objects are rejected during the deposition process, but the center-of-mass coordinates of the objects that will stay in the final configuration are still taken from a uniformly random distribution. Since needles have no width associated with them and they can be packed arbitrarily close to each other, the distribution of pairs of centers of masses (i.e., Ω) remains constant in q . We note that this result is in marked contrast to the FM, where a double-peak type of structure in Ω develops when clustering of fibers is enhanced in the limit $p \rightarrow 0$ [27].

2. Disks

The behavior of the pair distribution function must depend on q for objects with finite area. To illustrate this, we consider here the case of disks of radius r_d . In the RSA limit ($q = 1$), all objects are restricted not to be closer than twice the disk radius r_d . Thus, we can write the RSA approximation Ω_f in this limit as

$$\Omega_f(r) = C\theta(r - r_c)\Omega_a(r), \quad (13)$$

where $\theta(r)$ is the step function, and C a normalization constant. In Fig. 7(b) we show our numerical data for $\Omega(r)$, with $q = 0.9, 0.99, 0.999, \text{ and } 0.999$, and also the function $\Omega_f(r)$.

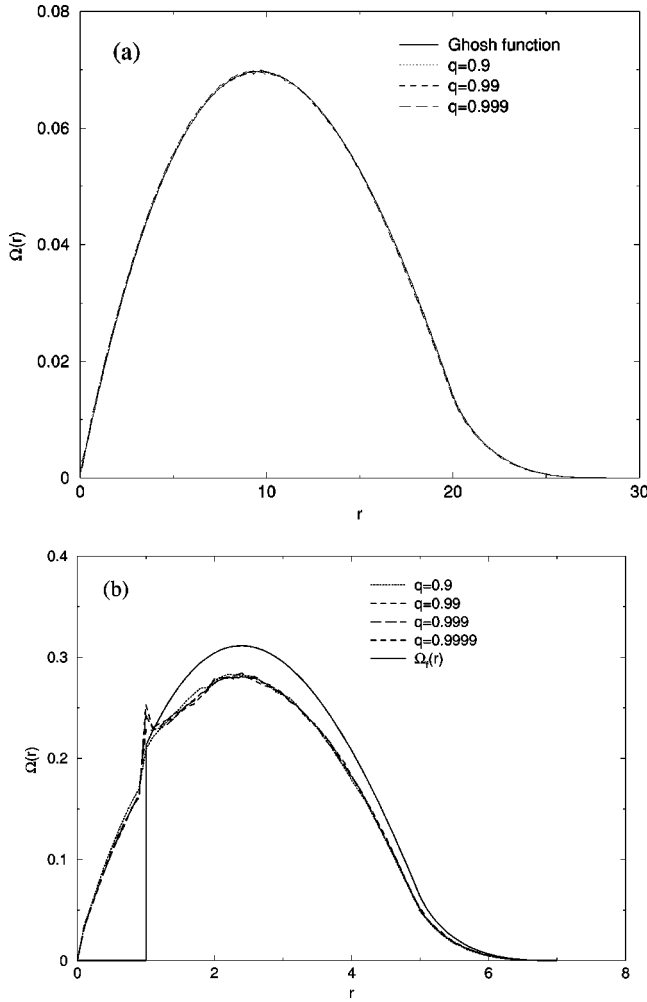


FIG. 7. Pair distribution functions for (a) needles of length $\lambda = 1$ and (b) disks of radius $r_d = 1/2$. See text for details.

In the limit of $q \rightarrow 1$, a cutoff in $\Omega(r)$ develops at $r_c = 2r_d$ corresponding to the nonoverlap condition. Following this, there is a sharp peak at $\Omega(r)$ just beyond r_c , where the disks are packed very closely together. We note that the approximation of Eq. (13) is unable to reproduce this peak, since the excess mass density cut off by the step function is uniformly distributed when $\Omega_f(r)$ is properly normalized.

B. The two-point mass density correlation function

The two-point mass density fluctuation correlation function is defined as

$$G(\vec{x}) \equiv \langle [m(\vec{x}') - \langle m \rangle][m(\vec{x}' + \vec{x}) - \langle m \rangle] \rangle, \quad (14)$$

where $m(\vec{x})$ is the mass density at \vec{x} , and $\langle m \rangle$ is the average mass density. This correlation function is a measure of the mass distribution in the network. We calculated $G(r)$ numerically by discretizing fibers on lattice points. The lattice model was solved with periodic boundary conditions and with the aspect ratio $\omega : \lambda : L = 2 : 20 : 150$, which is quite close to the needle limit. The lattice size was checked to be large enough so that finite size effects do not affect the correlation function in the range of interest.

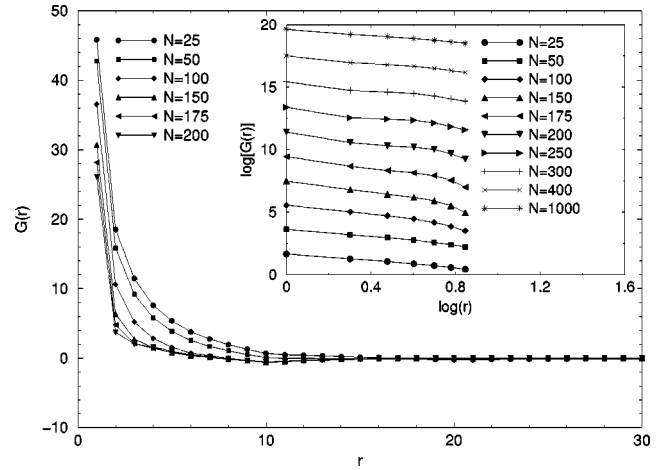


FIG. 8. The pair correlation function $G(r)$ for a discrete approximation of fibers ($\lambda/\omega = 20/2$) vs N for $q = 0.999$. The inset shows the initial power law type of decay of $G(r)$ for short distances $r < \lambda/2$.

In Fig. 8 we show a series of the functions for $q = 0.999$. As N increases toward $N_c \approx 200$, there is an increasing anticorrelation in $G(r)$ just beyond the fiber width $\omega = 2$. This reflects the effective repulsion and local alignment of anisotropic particles present in the model. Moreover, we find that $G(r)$ can be approximated by

$$G(r) \propto r^{-\alpha(N,q)} \text{ for } 0 < r < \Lambda(N,q), \quad (15)$$

where Λ is an effective cutoff for the power law form. Figure 9 shows the effective exponents $\alpha(N,q)$ vs N for the model for different values of q . For $q = 0$, $\alpha(N,0) \approx 1$ as expected [27]. The cutoff here is of the order of $\Lambda \approx \lambda/2$ for all values of N [4,27]. When q is close to unity, $\alpha(N,q)$ goes through a maximum as N increases. Moreover, Λ attains a minimum where α is maximum. This is again in contrast to the case of the FM, where the range of the approximate power law form was found to have a maximum close to the threshold, when clustering was enhanced [27]. We note that for $N \gg N_c$ the mass density of the networks again approaches the uniform distribution for any $q < 1$ [27].

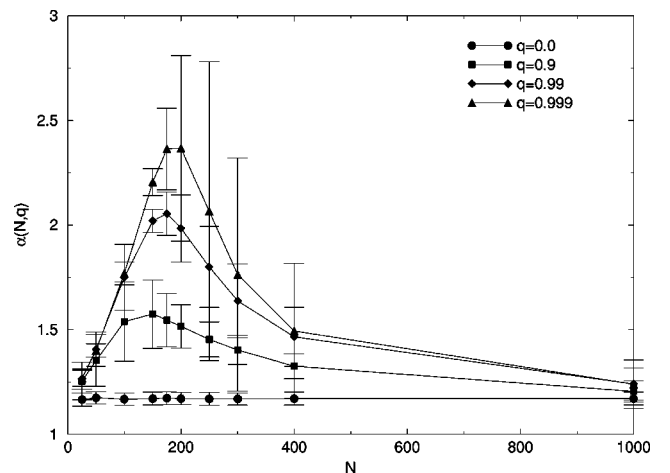


FIG. 9. The effective exponents of $G(r)$ vs N for various values of q . See text for details.

V. CONCLUSIONS AND DISCUSSION

In this work, we have presented a study of the percolation properties and spatial correlations in a simple 2D continuum deposition model, where there is a tunable interparticle contact repulsion. When this repulsion becomes strong, there are dramatic changes in the properties of the deposited networks. In particular, through a combination of numerical data and analytic arguments we have shown how for widthless needles the percolation threshold diverges in this limit. However, for objects with finite area there is just an increasing trend in the critical density. Interestingly enough, in the same limit the spatial pair distribution function shows no change for needles, but develops a finite cutoff radius for finite area

objects (disks). The effective repulsion and local ordering for anisotropic objects are also reflected in the mass density correlation function, which shows anticorrelation for densities near and below the critical density. Finally, we hope that the present results can be used in experimental studies of deposits of particles with repulsive interactions.

ACKNOWLEDGMENTS

We wish to thank M. Alava, M. Haataja, S. Majaniemi, and N. Provatas for technical assistance and useful discussions. This work has been supported in part by the Academy of Finland through the MATRA program.

-
- [1] J. W. Evans, *J. Math. Phys.* **65**, 1281 (1993).
- [2] V. Privman, in *Annual Reviews in Computational Physics*, Vol. 3, edited by D. Stauffer (World Scientific, Singapore, 1995).
- [3] G. Y. Onoda and E. G. Liniger, *Phys. Rev. A* **33**, 715 (1986); A. Schmit, R. Varoqui, S. Uniyal, J. L. Brash, and C. Pusiner, *J. Colloid Interface Sci.* **92**, 25 (1983); J. Feder and I. Giaever, *ibid.* **78**, 144 (1980).
- [4] M. Deng and C. T. J. Dodson, *Paper: An Engineered Stochastic Structure* (Tappi Press, Atlanta, GA, 1994).
- [5] K. J. Niskanen and M. J. Alava, *Phys. Rev. Lett.* **73**, 3475 (1994).
- [6] P. Nielaba and V. Privman, *Phys. Rev. E* **51**, 2022 (1995).
- [7] N. Ryde, H. Kihira, and E. Matijevic, *J. Colloid Interface Sci.* **151**, 421 (1992).
- [8] J. Vinnurva, M. J. Alava, T. Ala-Nissila, and J. Krug, *Phys. Rev. E* **58**, 1125 (1998).
- [9] A.-L. Barabasi and H. E. Stanley, *Fractal Concepts in Surface Growth* (Cambridge University Press, Cambridge, 1995).
- [10] C. A. Murray and D. G. Grier, *Am. Sci.* **83**, 238 (1995).
- [11] M. L. Kurnaz and J. V. Maher, *Phys. Rev. E* **53**, 978 (1996).
- [12] S. Schwarzer, *Phys. Rev. E* **52**, 6461 (1995).
- [13] G. E. Pike and C. H. Seager, *Phys. Rev. B* **10**, 1421 (1974).
- [14] I. Balberg and N. Binenbaum, *Phys. Rev. B* **28**, 3799 (1983).
- [15] P. C. Robinson, *J. Phys. A* **16**, 605 (1983).
- [16] I. Balberg, C. H. Anderson, S. Alexander, and N. Wagner, *Phys. Rev. B* **30**, 3933 (1984).
- [17] P. C. Robinson, *J. Phys. A* **17**, 2823 (1984).
- [18] A. L. R. Bug, S. A. Safran, and G. S. Grest, *Phys. Rev. Lett.* **55**, 1896 (1985).
- [19] I. Balberg, *Philos. Mag. B* **56**, 991 (1987).
- [20] D. Laría and F. Vericat, *Phys. Rev. B* **40**, 353 (1989).
- [21] S. B. Lee and S. Torquato, *Phys. Rev. A* **41**, 5338 (1990).
- [22] U. Alon, I. Balberg, and A. Drory, *Phys. Rev. Lett.* **66**, 2879 (1991).
- [23] C. Vanneste, A. Gilabert, and D. Sornette, *Phys. Lett. A* **155**, 174 (1991).
- [24] A. Drory, I. Balberg, and B. Berkowitz, *Phys. Rev. E* **49**, 949 (1994).
- [25] H. S. Choi, J. Talbot, G. Tarjus, and P. Viot, *Phys. Rev. E* **51**, 1353 (1995).
- [26] M. D. Rintoul and S. Torquato, *Phys. Rev. E* **52**, 2635 (1995).
- [27] N. Provatas, M. Haataja, E. Seppälä, S. Majaniemi, J. Åström, M. Alava, and T. Ala-Nissila, *J. Stat. Phys.* **87**, 385 (1997); *Physica A* **239**, 304 (1997).
- [28] N. Provatas, M. Haataja, J. Asikainen, S. Majaniemi, M. Alava, and T. Ala-Nissila, *Colloids Surf. A* (to be published).
- [29] J. Åström, Pro Gradu avhandling, Åbo Akademi, 1989 (unpublished).
- [30] N. Provatas, M. J. Alava, and T. Ala-Nissila, *Phys. Rev. E* **54**, R36 (1996).
- [31] W. J. Boudville and T. C. McGill, *Phys. Rev. B* **39**, 369 (1980).
- [32] N. Provatas, T. Ala-Nissila, and M. J. Alava, *Phys. Rev. Lett.* **75**, 3556 (1995).
- [33] D. Stauffer and A. Aharony, *Introduction to Percolation Theory* (Taylor and Francis, London, 1994).
- [34] We have checked the density profiles explicitly as a function of q and find that even near $q=1$, L' need not be larger than the largest object dimension.
- [35] J. Hoshen and R. Kopelman, *Phys. Rev. B* **14**, 3438 (1976).
- [36] P. J. Reynolds, H. E. Stanley, and W. Klein, *Phys. Rev. B* **21**, 1223 (1980).
- [37] The excluded volume $\langle A \rangle$ can be evaluated from Eq. (19) of Ref. [16] by using the present fiber dimensions and setting $\theta_\mu = \pi/2$.
- [38] O. J. Kallmes and H. Corte, *Tappi J.* **43**, 737 (1960).
- [39] R. M. Ziff and R. D. Vigil, *J. Phys. A* **23**, 5103 (1990).
- [40] We note that for the one-dimensional RSA, there is an exact result that $x = \sqrt{2} - 1 \approx 0.41$ [G. Tarjus and P. Viot, *Phys. Rev. Lett.* **67**, 1875 (1991)]. They conjecture that this result might hold for the 2D case as well.
- [41] B. Ghosh, *Bull. Calcutta Math. Soc.* **43**, 17 (1951).